

Mathematical Modeling of Tumor Vasculature/Angiogenesis

Subjects: Oncology

Contributor: David A. Hormuth, II

The recruitment of new vasculature via angiogenesis is a critical component of tumor development, which fundamentally influences tumor growth and response to treatment. The characterization of tumor-induced angiogenesis via mathematical models could enable approaches to forecast tumor response and improve patient care.

Keywords: computational oncology ; magnetic resonance imaging ; perfusion ; partial differential equations ; confocal microscopy ; systems biology ; treatment response ; vascular growth ; computational fluid

1. Introduction

In the early stages of tumor growth, a small population of tumor cells is supported by existing tissue vasculature and the diffusion of nutrients through the extravascular space. As this small population of tumor cells continues to grow, it may eventually reach a size where the diffusion of nutrients from existing vasculature is insufficient to support continued growth. Through the process of angiogenesis, new blood vessels are recruited from nearby vasculature to provide the crucial infrastructure needed to sustain further expansion of the tumor ^[1]. These three key points inform the foundation of many mathematical models of angiogenesis and arose from the seminal work on tumor angiogenesis by Folkman ^{[1][2]} and others ^{[3][4]} over the past half a century. Additional studies on angiogenic signaling ^{[5][6]} and vasculature properties ^{[4][7]} have also greatly influenced the development of a mathematical theory on angiogenesis. One notable observation was that compared to healthy appearing vasculature, tumor-associated vasculature has substantial structural and functional abnormalities characterized by non-hierarchical vessel networks, heterogeneous blood flow, and heterogeneous permeability ^{[4][7]}. These irregularities significantly influence the delivery of nutrients and removal of waste, while also having substantial implications on systemic and radiation therapy ^[8].

Quantitative and time-resolved imaging approaches, such as confocal imaging, photoacoustic imaging, and magnetic resonance imaging (MRI), could provide the necessary data to initialize, calibrate, and validate models of angiogenesis. Specifically, time-resolved imaging techniques of the vasculature have matured to the point where they can define or estimate subject-specific structural (e.g., vessel order and location) and functional (e.g., vessel permeability, blood flow) model parameters that would enable in silico investigations of tumor and vasculature dynamics ^[9].

The mathematical modeling of tumor angiogenesis at the cell scale has developed into a rich literature over the last few decades ^{[10][11][12][13][14][15]}. These models aim to give a rigorous mathematical description of tumor angiogenesis to enable the systematic investigation of the underlying biology that dictates vascular sprouting, perfusion, and response to therapy. By employing such models, it is possible to simulate and test scenarios in silico that are not easily tested experimentally. For example, comparing the limitless number of therapeutic regimens that can be constructed with varying dosing schedules and concentrations is experimentally intractable, but with a mathematical model these can be simulated and analyzed to select the optimal regimen ^[16].

2. Experimental Techniques across Scales

Figure 1 summarizes the cell to tissue scale approaches for imaging experiments, while **Table 1** lists the imaging techniques and the literature that integrates those techniques with mathematical theory at the cell and tissue scale.

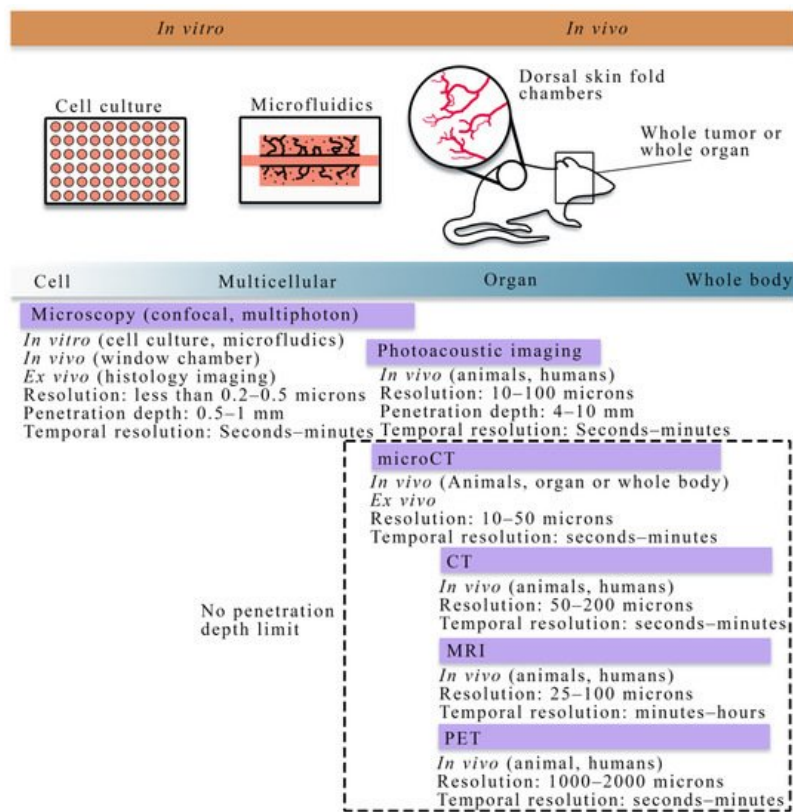


Figure 1. Overview of cell to tissue scale imaging. Experimental platforms from the cell to tissue scales consist of cell culture (to investigate cell dynamics), microfluidics (a perfused cell culture platform to observe angiogenesis), skin fold window chambers (an *in vivo* platform for optical imaging), and small animal or human whole organ and body imaging (for *in vivo* studies). Imaging techniques (purple bars) vary across spatial and temporal scales. *In vitro* imaging consists primarily of the microscopies (e.g., confocal, multiphoton). *In vivo* imaging is achievable with all the imaging techniques shown above; however, there are limitations in the penetration depth for microscopy and photoacoustic imaging. Magnetic resonance imaging (MRI), positron emission tomography (PET), and computed tomography (CT) are primarily *in vivo* techniques capable of whole animal or human imaging. Whole animal or body imaging is feasible with microCT, though it is typically used for whole organ or *ex vivo* imaging.

Table 1. Imaging techniques for visualizing vasculature and angiogenesis at cell scale and tissue scale.

Modality	Scale	Measurement	Uses in Literature
Microscopy (confocal, multiphoton, optical projection tomography, histology imaging)	Cell to tissue	Vascular structure, individual cell types, vessel porosity, flow	[17][18][19][20][21][22]
Photoacoustic imaging	Cell to tissue	Vascular structure, blood oxygenation	[23][24]
Angiography (X-ray, CT, MRI)	Tissue	Vascular structure	[25][26][27][28]
Dynamic contrast-enhanced MRI or CT	Tissue	Perfusion, permeability, blood volume fraction	[16][29][30][31][32]
PET	Tissue	Perfusion, permeability, blood volume fraction	[27][28]
microCT	Tissue	Vascular structure	[25][26][27][28]

2.1. Quantitative Techniques for Observing Tumor Vasculature and Angiogenesis at the Cellular Scale

At the cellular scale, microscopy is the dominant imaging technique for providing quantitative measurements of tumor vasculature with a spatial resolution on the order of microns. Confocal microscopy, combined with immunofluorescence staining, has been used to acquire high resolution, temporally resolved images of vascular structure in angiogenic and vasculogenic assays [33][34][35]. This technology allows for analyzing *in vitro* spatial distributions of fluorescently labeled cell lines and can be coupled with fluorescing microspheres to investigate vascular integrity, enabling the integration of quantitative fluorescence measurements with mathematical modeling. Furthermore, confocal microscopy has also been

utilized *in vivo* to investigate functional microcirculation [36] in tumor-associated vasculature, the effects of radiotherapy [37] on neovasculature, and the oxygen distribution [38][39] in dorsal skin fold chambers [40]. While intravital microscopy provides a high-resolution longitudinal analysis *in vivo*, the chamber may alter the tumor-vasculature dynamics and it is fundamentally limited in the length of study (generally 2–3 weeks), and the number of imaging time points. Multiphoton microscopy [41], in comparison to confocal microscopy, has improved depth penetration and confines excitation to the focal plane of the lens, thereby decreasing the photodamage to the tissue. For many biological applications, tissue depths of ~500 microns can be imaged over time [41].

In addition to microscopy, photoacoustic imaging offers high spatial resolution (10–100 microns) while also being able to reach tissue penetration depths of around 4–10 cm [42][43].

2.2. Quantitative Techniques for Observing Tumor Vasculature and Angiogenesis at the Tissue Scale

Ex vivo and *in vivo* imaging play a central role in understanding the morphology and function of tumor vasculature and angiogenesis. In particular, *ex vivo* imaging techniques, including histology imaging [44] and micro-CT [45][25][26], can quantify tumor microvasculature and angiogenesis on excised tissue specimens and serve as the gold standard measurement. Less invasive observations of tumor-associated vasculature can now be achieved thanks to the development of *in vivo* imaging techniques [46], such as x-ray [47] and computed tomography (CT) [48][49][50], positron emission tomography (PET) [51][52], MRI [49][53][54][55][56][57][58][59], and optical imaging [60][61]. There are two main classes of imaging techniques applied to studying tumor-associated vasculature: (1) angiography, which is a technique used to visualize the vasculature structure, and (2) functional techniques used to quantify the properties of the tissue and vasculature. In conventional planar x-ray angiography [47], the patient is catheterized so that an iodinated contrast agent can be administered intravenously and then observed with fluoroscopy, thereby enabling the observation of the vascular architecture. CT angiography is an extension of x-ray angiography that enables the visualization of vessel structures in 3D. CT angiography has been commonly used to identify the location and anatomy of tumor-associated vessels (especially for pancreatic tumors), which plays a valuable role on diagnosis and the management of chemotherapy and surgery [62][63][64]. Magnetic resonance angiography (MRA) is an alternative approach that does not use ionizing radiation and can be used to visualize blood vessels, especially large arteries and veins [53]. MRA techniques aim at enhancing the contrast between blood vessels and the background tissue based on either the effects of blood flow on MR signal or the injection of exogenous contrast agents, thereby allowing for the quantification of several morphological characteristics of the vasculature, such as vessel tortuosity, density, diameter, and branching patterns as well as feeding and draining vessels [65][66].

3. Approaches for Modeling Tumor Vasculature at the Cell Scale

3.1. Mathematical Modeling of Tumor Vasculature and Angiogenesis at the Cell Scale

Mathematical models of tumor angiogenesis vary in the extent of biological detail they characterize and can be summarized as discrete (treating endothelial cells and vasculature as individual objects), continuous (treating endothelial cells or vasculature as concentrations), or hybrid (combining methodology from both discrete and continuum theory) models. Discrete models may track all endothelial cells as individual agents, or simply tip endothelial cells or TECs (the cells responsible for directed migration in response to chemical stimuli). In discrete models, the vasculature changes through time based on sets of rules dictating cell behavior (e.g., whether a cell will divide or migrate). Continuum models are based on ordinary or partial differential equations (PDEs) that govern the behavior of the endothelial cells through time. Hybrid models couple these two theories by, for example, discretely characterizing the TECs and continuously modeling the overall vessel morphology through a PDE. We note that while hybrid models could refer to models that have a discrete and continuous component within the modeling framework (which would dictate a hybrid modeling approach), here, we define hybrid as utilizing both discrete and continuous methodologies specifically applied to model the vasculature. The reader is invited to refer to **Figure 2** throughout this section as it shows examples of these three modeling approaches. All three modeling approaches are typically used to study the migration and development of tumor-associated vasculature in response to external stimuli (e.g., chemical, mechanical) in conjunction with a model of tumor growth. A simulation of the process of angiogenesis typically begins with the stimulation of endothelial cells by tumor angiogenic factors (TAF, a continuous field of pro-angiogenic proteins secreted by tumor cells) that are either explicitly coupled to a model of tumor cell growth or assumed to have a fixed initial distribution. Directed movement of endothelial cells is then influenced by chemical gradients (i.e., TAF), gradients in fibronectin or insoluble extra-cellular matrix (ECM) (i.e., haptotaxis), and mechanical cues (i.e., mechanotaxis) [67][68].

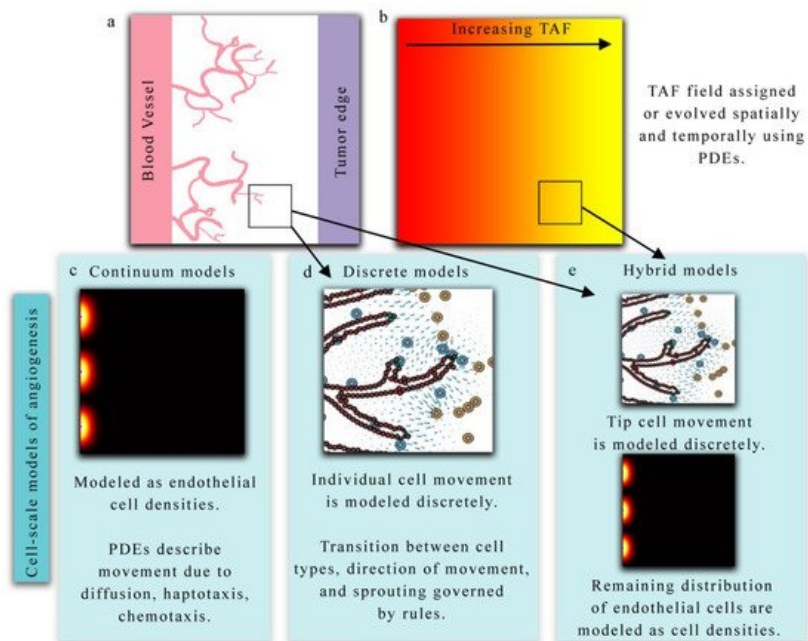


Figure 2. Overview of cell-scale models of angiogenesis. (Panels **a** and **b**) present a hypothetical biological scenario in which new vasculature is recruited via angiogenesis in response to tumor angiogenic factors (TAF) released by tumor cells. Continuum models (panel **c**) describe this phenomenon in terms of endothelial cell densities and the concentration of TAF. Partial differential equations (PDEs) provide a continuous representation of endothelial densities and often describe the spatial and temporal evolution via diffusion, haptotaxis, and chemotaxis terms. Alternatively, discrete models (panel **d**) can be used to explicitly describe the movement and behavior of each individual endothelial cell. Hybrid models (panel **e**) generally combine both discrete and continuum approaches to model TEC movement and endothelial cell densities, respectively, in response to TAF.

The continuum, discrete, and hybrid modeling approaches above provide complementary information on angiogenesis, and the choice of modeling approach is dependent on the desired goal or quantity of interest from the model itself. The primary advantage of using a continuous representation of tumor vasculature is the low computational cost, and the ability to utilize sophisticated parallel solvers for continuum equations. However, a continuum approach lacks the ability to resolve local key features of the changing vasculature including, for example, the activation of TECs (the cell responsible for directed migration) and the competition for the TEC phenotype among other TECs and neighboring endothelial cells. Discrete models can resolve these local features but become computationally expensive as the number of cells increase. Hybrid models balance both approaches and produce robust and sophisticated vascular fields, but often require complex numerical schemes to solve them. All three modeling approaches have been shown to qualitatively describe the dynamics of tumor angiogenesis; however, many parameters in these models are often assigned values without any experimental validation. This leads to models matching qualitative properties of angiogenesis such as TEC activation, sprout elongation, formation of anastomosis, and establishing blood flow, but have difficulty predicting actual experimental outcomes, since parameters are freely assigned. Recent advances, though, indicate that time-resolved quantitative imaging can provide the data necessary to inform and calibrate model parameters specific to the vasculature network under investigation.

3.2. Integrating Theory and Experimental Data at the Cellular Scale

Microfluidic devices are one promising platform that enable the culturing of tumor and/or endothelial cells in 2D or 3D, while simultaneously incorporating biochemical gradients, fluid flow, and mechanical signaling [69][70]. These devices can play a powerful role in the study of tumor angiogenesis and vasculature by providing a controlled, repeatable experimental platform in vitro that can isolate specific processes that are not easily studied individually in vivo. Many microfluidic devices are widely reproducible and allow for a systematic investigation of vasculogenesis [71][72][73][74], angiogenesis [75][76][77][78], and response to anti-angiogenic therapies [79].

While computational advances in discrete, continuum, and hybrid modeling along with experimental advances in microscopy and microfluidic devices have largely bridged this gap, significant progress in the rigorous integration of mathematical models of angiogenesis and experimental observations have yet to be realized at the cell scale. Phillips et al. [17][21][80] have proposed integrating confocal microscopy data from an in vitro vascularized tumor platform [78] with an agent-based mathematical model of tumor angiogenesis [80]. In their framework, time-resolved confocal measurements of individual angiogenic sprouts are used to calibrate and validate a multiscale agent-based model. The agent-based model

captures the dynamics of endothelial cells. Each agent represents a single endothelial cell that can be in one of the following phenotypes: tip, stalk, or phalanx cell [81]. Tumor cells release TAF, which is modeled by a reaction-diffusion equation and is responsible for guiding the movement and phenotypic transitions of endothelial cells. In their preliminary study [21], they calibrated the endothelial cell cycle duration and TEC velocity and used these parameters to estimate the total sprout length at the end of the imaging experiment. Phillips et al. [21] observed a 12.5% error in sprout length between the model and the image measurement. Future efforts are aimed at improving the spatial agreement between the model and the measurements. **Table 2** summarizes the literature reviewed in this section and how the selected models are integrated with imaging data.

Table 2. Examples of studies integrating imaging data with mathematical modeling at the cell scale.

Paper	Modeling Approach	Scale	Use of Data
Perfahl 2011 [18]	Discrete	Cell-tissue	Microscopy used to initialize vasculature network
Xu 2020 [23]	Hybrid	Cell-tissue	Photoacoustic imaging was used to initialize vasculature network
Stepanova 2021 [19]	Hybrid	Cell	Agent-based model was calibrated against in vitro assays
Phillips 2019,2020 [17][21][80]	Discrete	Cell	Time-resolved microscopy was used to initialize and calibrate an agent-based model

4. Approaches for Modeling Tumor Vasculature and Angiogenesis at the Tissue Scale

4.1. Mathematical Modeling of Tumor Vasculature and Angiogenesis at the Tissue Scale

4.1.1. Models of Evolving Tumor Vascular Network

The first area Figure 4 of focus (panel a in **Figure 3**) bridges the cell to tissue scale by modeling the formation and evolution of tumor-induced angiogenic networks which are predominately modeled using a discrete (lattice-based and lattice-free). Discrete approaches typically model individual TEC movement, while continuous approaches model the change in a spatially averaged, continuous variable (e.g., vasculature density or vascular volume fraction). Hybrid approaches combine the discrete and continuous approaches to provide a spatially resolved vasculature network, which can be mapped to a continuous domain to facilitate interaction with continuous elements of their mathematical modeling system (e.g., TAF or nutrients). One representative example by Frieboes et al. [67] applies a hybrid approach to describe angiogenesis coupled to tumor growth.

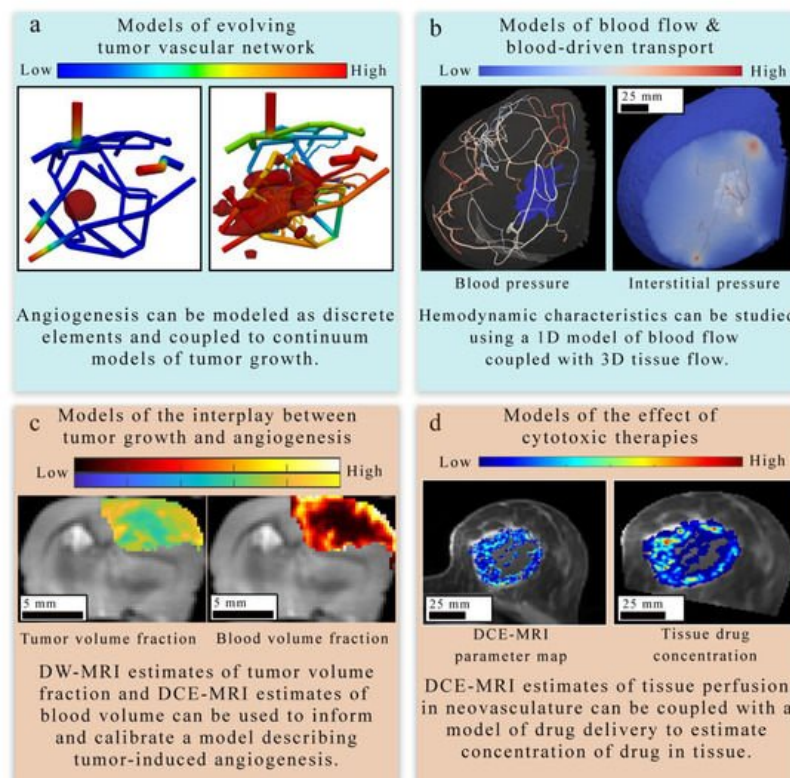


Figure 3. Overview of tissue-scale models of angiogenesis and vasculature. There are four main approaches to modeling tumor-induced angiogenesis and vasculature at the tissue scale level. (Panel **a**) provides an example of a discrete modeling approach [82][83] used to describe the evolving geometry of tumor vasculature in response to tumor growth. This simulation employs a 3D continuous multi-species tumor growth model coupled to a 1D discrete model of angiogenesis. The tissue domain initially features a small spherical tumor core, which grows in response to the changing vasculature network. The colors in the network show the nutrient volume fraction. (Panel **b**) displays how the function of existing tumor vasculature in the breast can be studied with computational fluid dynamics [30] to estimate hemodynamic properties of the vascular network. In (panel **c**), diffusion weighted (DW-) and DCE-MRI acquired in a murine brain tumor model (C6 glioma) are used to provide tumor volume fraction and blood volume fraction estimates to initialize and calibrate a model of tumor-induced angiogenesis. The model derived estimates of tumor and blood volume fraction are overlaid on an axial T_2 -weighted MRI through the center slice of the tumor. A coupled set of PDEs [29] are used to describe the proliferation, diffusion and death of tumor cells and the angiogenesis, diffusion, and regression of the vasculature. In (panel **d**), estimates of tissue perfusion in the breast derived from quantitative imaging are coupled with a mathematical model of drug delivery [32] and tumor growth to observe the effect of tumor vasculature on drug distribution and tumor response to treatment. Both the left and right images in (panel **d**) show quantitative maps of DCE-MRI parameters or drug concentration overlaid on an anatomical image acquired in the same plane. The right drug concentration map is an enlargement of the computational domain.

4.1.2. Models of Blood Flow and Blood-Driven Transport

The second area (panel b in Figure 4) focuses on estimating blood flow and transport within the vasculature and through the interstitial space. In discrete vascular models both the pre-existing and the angiogenic vasculature are frequently approximated by a 1D network of connected straight cylinders with the flow in each cylinder simulated using the 1D Poiseuille law [30][67][68][82][83][84][85][86][87]. In continuous vascular flow models the vasculature is described with a spatially averaged, continuous variable (e.g., vasculature density or vascular volume fraction), and the transport of the substance of interest (e.g., drug or nutrient) through the interstitial space is described with a reaction-diffusion-advection model [88][89][90][91] describing the delivery, diffusion, and the transport of that substance due to bulk fluid flow. Hybrid vascular flow models [92][93][94] combine the discrete and continuum approaches; capillaries and smaller vessels are approximated with a continuum approach, whereas the large vessels are explicitly retained, and their flow is simulated as in discrete models.

4.1.3. Models of Tumor and Vasculature Growth and Response to Therapy

The third and fourth areas focus on describing the mechanisms underlying the complex interplay between tumor growth and vasculature in the absence of treatment (panel c in Figure 4) [29][23][67][68][95][83][88][89] and during treatment (panel d in Figure 4).

At the tissue scale, models of tumor cell dynamics are typically captured in a continuous fashion by means of a PDE system [96][97][98][99]. This is most commonly achieved through either reaction-diffusion-advection equations or phase-field equations. Reaction-diffusion-advection equations describe the spatiotemporal dynamics of cell density (or tumor volume fraction) as a combination of random movement of cells via diffusion, directed movement of cells via advection, and reaction terms representing (for example) tumor cell proliferation, apoptosis, and cytotoxic effects due to treatments [29][32][92][88][89][91][98].

4.2. Integrating Theory and Experimental Data at the Tissue Scale

Recent studies have proposed several promising approaches for integrating mathematical models with experimental imaging data at both the pre-clinical and clinical levels. The reader is referred to **Table 3** for a summary of these approaches and the type of data used to inform the model.

Table 3. Examples of studies integrating imaging data with mathematical modeling at the tissue scale.

Paper	Modeling Approach	Scale	Use of Data
d'Esposito 2018 [22]	Continuum	Tissue	Whole tumor imaging was used to initialize vasculature network, perfusion model validated against DCE-MRI
Stamatelos 2019 [26]	Continuum	Tissue	Whole tumor microscopy was used to initialize tumor vasculature
Adhikarla 2012, 2016 [27][28]	Discrete	Tissue	CT data was used to initialize vasculature network, model parameters were calibrated against PET measures of hypoxia
Wu 2020 [30]	Continuum	Tissue	DCE-MRI used to initialize breast vasculature

Paper	Modeling Approach	Scale	Use of Data
Titz 2012 ^[100]	Continuum	Cell-Tissue	PET estimates of oxygenation and proliferation were used to initialize tumor simulation and calibrate model parameters
Hormuth 2019,2020 ^{[29][31]}	Continuum	Tissue	Time-resolved DCE-MRI to calibrate and validate models
Jarrett 2018, 2020 ^{[16][32]}	Continuum	Tissue	Time-resolved DCE-MRI used to estimate drug delivery

4.2.1. Applications to Estimate Perfusion and Delivery

Recent studies have provided important foundations on integrating imaging measurements of tumor-associated vasculature with mathematical models, which can provide a means to rigorously understand and predict tumor blood flow, interstitial transport, and angiogenesis. For example, d'Esposito et al. ^[22] performed fluorescence imaging to visualize tumor microvasculature in fixed tumor samples to inform a model of tumor perfusion. The segmented microvasculature was used to initialize the vasculature network for a computational fluid dynamic (CFD) model describing steady-state blood and interstitial flow. Using the CFD model, the authors estimated interstitial fluid pressure and velocity, blood flow and pressure, and the delivery of a widely used MRI contrast agent. Their CFD model predicted a heterogeneous spatial distribution of the contrast agent, which was validated against in vivo DCE-MRI.

4.2.2. Applications to Treatment Response

The treatment efficacy of systemic therapies administered intravenously relies on the delivery of drugs through the bloodstream, which is highly dependent on the vascular structure and associated perfusion. Additionally, multiple pre-clinical and clinical studies have shown that anti-VEGF therapy changes tumor vasculature towards a more “mature” or “normal” phenotype, thereby improving the delivery and efficacy of concomitant chemotherapies ^[101]. Therefore, the use of data-driven modeling to evaluate angiogenesis is a promising means to assess and predict tumor response to therapies. The approach proposed by Titz et al. ^[100] employed a continuum model to simulate tumor and vasculature responses to anti-angiogenic therapy. Pre-treatment PET measurements of cellular proliferation and hypoxia were used to initialize the simulation and estimate model parameters. In their simulations, hypoxic tumors released TAF or VEGF to stimulate endothelial cell proliferation and an increase in microvessel density. The estimated microvessel density was used to estimate the average voxel oxygenation. The model parameters describing cellular and vascular proliferation were adjusted to minimize the error between the measured oxygenation from PET and the model-estimated oxygenation. Using this modeling framework, the authors estimated the response to anti-angiogenic therapy and demonstrated that anti-angiogenic therapy could be personalized based on the initial levels of VEGF within the tumor.

5. Conclusions

In summary, the integration of biologically-based mathematical modeling of tumor vasculature and angiogenesis with time-resolved experimental data promises to enable further understandings of angiogenesis from the cell to tissue scales. Models validated by experimental data, could then be used to generate testable hypotheses or predict the spatial-temporal evolution of the tumor and its associated vasculature. Furthermore, at the clinical level mathematical models initialized and constrained by quantitative imaging techniques could produce timely and actionable forecasts of tumor growth and response that could help guide clinical decisions and fundamentally improve patient care.

References

- Folkman, J.; Bach, M.; Rowe, J.W.; Davidoff, F.; Lambert, P.; Hirsch, C.; Goldberg, A.; Hiatt, H.H.; Glass, J.; Henshaw, E. Tumor Angiogenesis—Therapeutic Implications. *N. Engl. J. Med.* 1971, 285, 1182–1186.
- Folkman, J. Tumor Angiogenesis; Klein, G., Weinhouse, S., Haddow, A.B.T.-A., Eds.; Academic Press: Cambridge, MA, USA, 1974; Volume 19, pp. 331–358. ISBN 0065230X.
- Carmeliet, P. Angiogenesis in health and disease. *Nat. Med.* 2003, 9, 653–660.
- Jain, R.K.; di Tomaso, E.; Duda, D.G.; Loeffler, J.S.; Sorensen, A.G.; Batchelor, T.T. Angiogenesis in brain tumours. *Nat. Rev. Neurosci.* 2007, 8, 610–622.
- Folkman, J. Angiogenesis in cancer, vascular, rheumatoid and other disease. *Nat. Med.* 1995, 1, 27–30.

6. Plate, K.H.; Breier, G.; Weich, H.A.; Risau, W. Vascular endothelial growth factor is a potential tumour angiogenesis factor in human gliomas in vivo. *Nature* 1992, 359, 845–848.
7. Carmeliet, P. Angiogenesis in life, disease and medicine. *Nature* 2005, 438, 932–936.
8. Gillies, R.J.; Schornack, P.A.; Secomb, T.W.; Raghunand, N. Causes and effects of heterogeneous perfusion in tumors. *Neoplasia* 1999, 1, 197–207.
9. Hormuth, D.A.; Jarrett, A.M.; Lorenzo, G.; Ernesto, A.B.F.; Wu, C.; Chung, C.; Patt, D.; Yankeelov, T.E.; Hormuth, D.A.; Jarrett, A.M.; et al. Math, magnets, and medicine: Enabling personalized oncology. *Expert Rev. Precis. Med. Drug Dev.* 2021, 6, 79–81.
10. Chaplain, M.A.J.; McDougall, S.R.; Anderson, A.R.A. Mathematical modeling of tumor-induced angiogenesis. *Annu. Rev. Biomed. Eng.* 2006, 8, 233–257.
11. Anderson, A.R.A.; Chaplain, M.A.J. Continuous and discrete mathematical models of tumor-induced angiogenesis. *Bull. Math. Biol.* 1998, 60, 857–899.
12. Yankeelov, T.E.; An, G.; Saut, O.; Luebeck, E.G.; Popel, A.S.; Ribba, B.; Vicini, P.; Zhou, X.; Weis, J.A.; Ye, K.; et al. Multi-scale Modeling in Clinical Oncology: Opportunities and Barriers to Success. *Ann. Biomed. Eng.* 2016, 44, 2626–2641.
13. Jarrett, A.M.; Lima, E.A.B.F.; Hormuth, D.A.; McKenna, M.T.; Feng, X.; Ekrut, D.A.; Resende, A.C.M.; Brock, A.; Yankeelov, T.E. Mathematical models of tumor cell proliferation: A review of the literature. *Expert Rev. Anticancer Ther.* 2018, 18, 1271–1286.
14. Sun, X.; Zhang, L.; Tan, H.; Bao, J.; Strouthos, C.; Zhou, X. Multi-scale agent-based brain cancer modeling and prediction of TKI treatment response: Incorporating EGFR signaling pathway and angiogenesis. *BMC Bioinform.* 2012, 13, 218.
15. Olsen, M.M.; Siegelmann, H.T. Multiscale agent-based model of tumor angiogenesis. *Procedia Comput. Sci.* 2013, 18, 1016–1025.
16. Jarrett, A.M.; Hormuth, D.A.; Wu, C.; Syed, A.K.; Virostko, J.; Sorace, A.; DiCarlo, J.C.; Kowalski, J.; Patt, D.; Goodgame, B.; et al. Evaluating patient-specific neoadjuvant regimens for breast cancer via a mathematical model constrained by quantitative magnetic resonance imaging data. *Neoplasia* 2020, 22, 820–830.
17. Kazerouni, A.S.; Gadde, M.; Gardner, A.; Hormuth, D.A.; Jarrett, A.M.; Johnson, K.E.; Lima, E.A.B.F.; Lorenzo, G.; Phillips, C.; Brock, A.; et al. Integrating quantitative assays with biologically-based mathematical modeling for predictive oncology. *iScience* 2020, 23, 101807.
18. Perfahl, H.; Byrne, H.M.; Chen, T.; Estrella, V.; Alarcón, T.; Lapin, A.; Gatenby, R.A.; Gillies, R.J.; Lloyd, M.C.; Maini, P.K.; et al. Multiscale Modelling of Vascular Tumour Growth in 3D: The Roles of Domain Size and Boundary Conditions. *PLoS ONE* 2011, 6, e14790.
19. Stepanova, D.; Byrne, H.M.; Maini, P.K.; Alarcon, T. A multiscale model of complex endothelial cell dynamics in early angiogenesis. *PLoS Comput. Biol.* 2021, 17, 1–44.
20. Jakobsson, L.; Franco, C.A.; Bentley, K.; Collins, R.T.; Ponsioen, B.; Aspalter, I.M.; Rosewell, I.; Busse, M.; Thurston, G.; Medvinsky, A.; et al. Endothelial cells dynamically compete for the tip cell position during angiogenic sprouting. *Nat. Cell Biol.* 2010, 12, 943–953.
21. Gadde, M.; Lima, E.A.B.F.; Phillips, C.M.; Rylander, M.N.; Yankeelov, T.E. A multi-scale model of tumor growth and angiogenesis calibrated by data from a tissue-mimicking, 3D, microfluidic platform. In *Proceedings of the Cancer Research UK-AACR Joint Conference on Engineering and Physical Sciences in Oncology*, London, England, 15–17 October 2019.
22. D'Esposito, A.; Sweeney, P.W.; Ali, M.; Saleh, M.; Ramasawmy, R.; Roberts, T.A.; Agliardi, G.; Desjardins, A.; Lythgoe, M.F.; Pedley, R.B.; et al. Computational fluid dynamics with imaging of cleared tissue and of in vivo perfusion predicts drug uptake and treatment responses in tumours. *Nat. Biomed. Eng.* 2018, 2, 773–787.
23. Xu, J.; Vilanova, G.; Gomez, H. Phase-field model of vascular tumor growth: Three-dimensional geometry of the vascular network and integration with imaging data. *Comput. Methods Appl. Mech. Eng.* 2020, 359, 112648.
24. Vilanova, G.; Burés, M.; Colominas, I.; Gomez, H. Computational modelling suggests complex interactions between interstitial flow and tumour angiogenesis. *J. R. Soc. Interface* 2018, 15, 20180415.
25. Stamatelos, S.K.; Kim, E.; Pathak, A.P.; Popel, A.S. A bioimage informatics based reconstruction of breast tumor microvasculature with computational blood flow predictions. *Microvasc. Res.* 2014, 91, 8–21.
26. Stamatelos, S.K.; Bhargava, A.; Kim, E.; Popel, A.S.; Pathak, A.P. Tumor Ensemble-Based Modeling and Visualization of Emergent Angiogenic Heterogeneity in Breast Cancer. *Sci. Rep.* 2019, 9, 5276.

27. Vikram, A.; Robert, J. An imaging-based stochastic model for simulation of tumour vasculature. *Phys. Med. Biol.* 2012, 57, 6103.
28. Adhikarla, V.; Jeraj, R. An imaging-based computational model for simulating angiogenesis and tumour oxygenation dynamics. *Phys. Med. Biol.* 2016, 61, 3885–3902.
29. Hormuth, D.A.; Jarrett, A.M.; Feng, X.; Yankeelov, T.E. Calibrating a Predictive Model of Tumor Growth and Angiogenesis with Quantitative MRI. *Ann. Biomed. Eng.* 2019, 47, 1539–1551.
30. Wu, C.; Hormuth, D.A.; Oliver, T.A.; Pineda, F.; Lorenzo, G.; Karczmar, G.S.; Moser, R.D.; Yankeelov, T.E. Patient-Specific Characterization of Breast Cancer Hemodynamics Using Image-Guided Computational Fluid Dynamics. *IEEE Trans. Med. Imaging* 2020, 39, 2760–2771.
31. Hormuth, D.A.; Jarrett, A.M.; Yankeelov, T.E. Forecasting tumor and vasculature response dynamics to radiation therapy via image based mathematical modeling. *Radiat. Oncol.* 2020, 15, 4.
32. Jarrett, A.; Hormuth, D., II; Barnes, S.; Feng, X.; Huang, W.; Yankeelov, T. Incorporating drug delivery into an imaging-driven, mechanics-coupled reaction diffusion model for predicting the response of breast cancer to neoadjuvant chemotherapy: Theory and preliminary clinical results. *Phys. Med. Biol.* 2018, 63, 105015.
33. Gurcan, M.N.; Boucheron, L.E.; Can, A.; Madabhushi, A.; Rajpoot, N.M.; Yener, B. Histopathological Image Analysis: A Review. *IEEE Rev. Biomed. Eng.* 2009, 2, 147–171.
34. Heindl, A.; Nawaz, S.; Yuan, Y. Mapping spatial heterogeneity in the tumor microenvironment: A new era for digital pathology. *Lab. Investig.* 2015, 95, 377–384.
35. Saucedo, A.M.; De La Cerda, J.; Suami, H.; Serda, R.E. Multimodal imaging of the tumor microenvironment and biological responses to immune therapy. *Biomed. Microdevices* 2018, 20, 105.
36. Wu, N.Z.; Klitzman, B.; Rosner, G.; Needham, D.; Dewhirst, M.W. Measurement of material extravasation in microvascular networks using fluorescence video-microscopy. *Microvasc. Res.* 1993, 46, 231–253.
37. Hori, K.; Saito, S.; Tamai, M. Effect of irradiation on neovascularization in rat skinfold chambers: Implications for clinical trials of low-dose radiotherapy for wet-type age-related macular degeneration. *Int. J. Radiat. Oncol. Biol. Phys.* 2004, 60, 1564–1571.
38. Dewhirst, M.W.; Ong, E.T.; Braun, R.D.; Smith, B.; Klitzman, B.; Evans, S.M.; Wilson, D. Quantification of longitudinal tissue pO₂ gradients in window chamber tumours: Impact on tumour hypoxia. *Br. J. Cancer* 1999, 79, 1717–1722.
39. Dewhirst, M.W.; Ong, E.T.; Klitzman, B.; Secomb, T.W.; Vinuya, R.Z.; Dodge, R.; Brizel, D.; Gross, J.F. Perivascular oxygen tensions in a transplantable mammary tumor growing in a dorsal flap window chamber. *Radiat. Res.* 1992, 130, 171.
40. Koehl, G.E.; Gaumann, A.; Geissler, E.K. Intravital microscopy of tumor angiogenesis and regression in the dorsal skin fold chamber: Mechanistic insights and preclinical testing of therapeutic strategies. *Clin. Exp. Metastasis* 2009, 26, 329–344.
41. Tozer, G.M.; Ameer-Beg, S.M.; Baker, J.; Barber, P.R.; Hill, S.A.; Hodgkiss, R.J.; Locke, R.; Prise, V.E.; Wilson, I.; Vojnovic, B. Intravital imaging of tumour vascular networks using multi-photon fluorescence microscopy. *Adv. Drug Deliv. Rev.* 2005, 57, 135–152.
42. Brown, E.; Brunker, J.; Bohndiek, S.E. Photoacoustic imaging as a tool to probe the tumour microenvironment. *DMM Dis. Model. Mech.* 2019, 12, dmm039636.
43. Jathoul, A.P.; Laufer, J.; Ogunlade, O.; Treeby, B.; Cox, B.; Zhang, E.; Johnson, P.; Pizzey, A.R.; Philip, B.; Marafioti, T.; et al. Deep in vivo photoacoustic imaging of mammalian tissues using a tyrosinase-based genetic reporter. *Nat. Photonics* 2015, 9, 239–246.
44. Fox, S.B.; Harris, A.L. Histological quantitation of tumour angiogenesis. *APMIS* 2004, 112, 413–430.
45. Ehling, J.; Theek, B.; Gremse, F.; Baetke, S.; Möckel, D.; Maynard, J.; Ricketts, S.A.; Grüll, H.; Neeman, M.; Knuechel, R.; et al. Micro-CT imaging of tumor angiogenesis: Quantitative measures describing micromorphology and vascularization. *Am. J. Pathol.* 2014, 184, 431–441.
46. McDonald, D.M.; Choyke, P.L. Imaging of angiogenesis: From microscope to clinic. *Nat. Med.* 2003, 9, 713–725.
47. Iwazawa, J.; Ohue, S.; Mitani, T.; Abe, H.; Hashimoto, N.; Hamuro, M.; Nakamura, K. Identifying feeding arteries during TACE of hepatic tumors: Comparison of C-Arm CT and digital subtraction angiography. *Am. J. Roentgenol.* 2009, 192, 1057–1063.
48. Drescher, R.; Freesmeyer, M. PET angiography: Application of early dynamic PET/CT to the evaluation of arteries. *Am. J. Roentgenol.* 2013, 201, 908–911.

49. Cuenod, C.A.; Fournier, L.; Balvay, D.; Guinebretière, J.M. Tumor angiogenesis: Pathophysiology and implications for contrast-enhanced MRI and CT assessment. *Abdom. Imaging* 2006, 31, 188–193.
50. Soriano, A.; Castells, A.; Ayuso, C.; Ayuso, J.R.; De Caralt, M.T.; Ginès, M.À.; Real, M.I.; Gilabert, R.; Quintó, L.; Trilla, A.; et al. Preoperative Staging and Tumor Resectability Assessment of Pancreatic Cancer: Prospective Study Comparing Endoscopic Ultrasonography, Helical Computed Tomography, Magnetic Resonance Imaging, and Angiography. *Am. J. Gastroenterol.* 2004, 99, 492–501.
51. Mullani, N.A.; Herbst, R.S.; O'Neil, R.G.; Gould, K.L.; Barron, B.J.; Abbruzzese, J.L. Tumor blood flow measured by PET dynamic imaging of first-pass 18F-FDG uptake: A comparison with 15O-labeled water-measured blood flow. *J. Nucl. Med.* 2008, 49, 517–523.
52. Massaro, A.; Ferretti, A.; Secchiero, C.; Cittadin, S.; Milan, E.; Tamiso, L.; Pavan, L.; Tommasi, E.; Marzola, M.C.; Chondrogiannis, S.; et al. Optimising 18F-Choline PET/CT acquisition protocol in prostate cancer patients. *N. Am. J. Med. Sci.* 2012, 4, 416–420.
53. Van Vliet, M.; Van Dijke, C.F.; Wielopolski, P.A.; Ten Hagen, T.L.M.; Veenland, J.F.; Preda, A.; Loeve, A.J.; Eggermont, A.M.M.; Krestin, G.P. MR angiography of tumor-related vasculature: From the clinic to the microenvironment. *Radiographics* 2005, 25, 85–98.
54. Brubaker, L.M.; Bullitt, E.; Yin, C.; Van Dyke, T.; Lin, W. Magnetic resonance angiography visualization of abnormal tumor vasculature in genetically engineered mice. *Cancer Res.* 2005, 65, 8218–8223.
55. Bullitt, E.; Zeng, D.; Gerig, G.; Aylward, S.; Joshi, S.; Smith, J.K.; Lin, W.; Ewend, M.G. Vessel tortuosity and brain tumor malignancy: A blinded study. *Proc. Acad. Radiol.* 2005, 12, 1232–1240.
56. Neves, F.; Huwart, L.; Jourdan, G.; Reizine, D.; Herman, P.; Vicaut, E.; Guichard, J.P. Head and neck paragangliomas: Value of contrast-enhanced 3D MR angiography. *Proc. Am. J. Neuroradiol.* 2008, 29, 883–889.
57. Fuss, M.; Wenz, F.; Essig, M.; Muentner, M.; Debus, J.; Herman, T.S.; Wannemacher, M. Tumor angiogenesis of low-grade astrocytomas measured by dynamic susceptibility contrast-enhanced MRI (DSC-MRI) is predictive of local tumor control after radiation therapy. *Int. J. Radiat. Oncol. Biol. Phys.* 2001, 51, 478–482.
58. Kickingereder, P.; Brugnara, G.; Hansen, M.B.; Nowosielski, M.; Pflüger, I.; Schell, M.; Isensee, F.; Foltyn, M.; Neuberger, U.; Kessler, T.; et al. Noninvasive characterization of tumor angiogenesis and oxygenation in bevacizumab-treated recurrent glioblastoma by using dynamic susceptibility MRI: Secondary analysis of the European Organization for Research and Treatment of Cancer 26101 Trial. *Radiology* 2020, 297, 164–175.
59. Puig, J.; Blasco, G.; Daunis-i-Estadella, J.; Alberich-Bayarri, A.; Essig, M.; Jain, R.; Remollo, S.; Hernández, D.; Puigdemont, M.; Sánchez-González, J.; et al. High-resolution blood-pool-contrast-enhanced MR angiography in glioblastoma: Tumor-associated neovascularization as a biomarker for patient survival. A preliminary study. *Neuroradiology* 2016, 58, 17–26.
60. Cai, W.; Shin, D.W.; Chen, K.; Gheysens, O.; Cao, Q.; Wang, S.X.; Gambhir, S.S.; Chen, X. Peptide-labeled near-infrared quantum dots for imaging tumor vasculature in living subjects. *Nano Lett.* 2006, 6, 669–676.
61. Senarathna, J.; Prasad, A.; Bhargava, A.; Gil, S.; Thakor, N.V.; Pathak, A.P. HemoSYS: A Toolkit for Image-based Systems Biology of Tumor Hemodynamics. *Sci. Rep.* 2020, 10, 2372.
62. Sze, D.Y.; Razavi, M.K.; So, S.K.S.; Jeffrey, J. Impact of multidetector CT hepatic arteriography on the planning of chemoembolization treatment of hepatocellular carcinoma. *Am. J. Roentgenol.* 2001, 177, 1339–1345.
63. Fishman, E.K.; Horton, K.M. Imaging Pancreatic Cancer: The Role of Multidetector CT with Three-Dimensional CT Angiography. *Pancreatol.* 2001, 1, 610–624.
64. Horton, K.M.; Fishman, E.K. Volume-rendered 3D CT of the mesenteric vasculature: Normal anatomy, anatomic variants, and pathologic conditions. *Radiographics* 2002, 22, 161–172.
65. Bullitt, E.; Gerig, G.; Pizer, S.M.; Lin, W.; Aylward, S.R. Measuring Tortuosity of the Intracerebral Vasculature from MRA Images. *IEEE Trans. Med. Imaging* 2003, 22, 1163–1171.
66. Mustafi, D.; Leinroth, A.; Fan, X.; Markiewicz, E.; Zamora, M.; Mueller, J.; Conzen, S.D.; Karczmar, G.S. Magnetic resonance angiography shows increased arterial blood supply associated with murine mammary cancer. *Int. J. Biomed. Imaging* 2019, 2019.
67. Frieboes, H.B.; Jin, F.; Chuang, Y.-L.; Wise, S.M.; Lowengrub, J.S.; Cristini, V. Three-dimensional multispecies nonlinear tumor growth-II: Tumor invasion and angiogenesis. *J. Theor. Biol.* 2010, 264, 1254–1278.
68. Vavourakis, V.; Wijeratne, P.A.; Shipley, R.; Loizidou, M.; Stylianopoulos, T.; Hawkes, D.J. A Validated Multiscale In-Silico Model for Mechano-sensitive Tumour Angiogenesis and Growth. *PLoS Comput. Biol.* 2017, 13, e1005259.
69. Meyvantsson, I.; Beebe, D.J. Cell culture models in microfluidic systems. *Annu. Rev. Anal. Chem.* 2008, 1, 423–449.

70. Wang, X.; Sun, Q.; Pei, J. Microfluidic-based 3D engineered microvascular networks and their applications in vascularized microtumor models. *Micromachines* 2018, 9, 493.
71. Hsu, Y.H.; Moya, M.L.; Hughes, C.C.W.; George, S.C.; Lee, A.P. A microfluidic platform for generating large-scale nearly identical human microphysiological vascularized tissue arrays. *Lab Chip* 2013, 13, 2990–2998.
72. Hsu, Y.H.; Moya, M.L.; Abiri, P.; Hughes, C.C.W.; George, S.C.; Lee, A.P. Full range physiological mass transport control in 3D tissue cultures. *Lab Chip* 2013, 13, 81–89.
73. Moya, M.L.; Hsu, Y.H.; Lee, A.P.; Christopher, C.W.H.; George, S.C. In vitro perfused human capillary networks. *Tissue Eng. Part C Methods* 2013, 19, 730–737.
74. Raghavan, S.; Nelson, C.M.; Baranski, J.D.; Lim, E.; Chen, C.S. Geometrically controlled endothelial tubulogenesis in micropatterned gels. *Tissue Eng. Part A* 2010, 16, 2255–2263.
75. Vickerman, V.; Kamm, R.D. Mechanism of a flow-gated angiogenesis switch: Early signaling events at cell-matrix and cell-cell junctions. *Integr. Biol.* 2012, 4, 863–874.
76. Shin, Y.; Jeon, J.S.; Han, S.; Jung, G.S.; Shin, S.; Lee, S.H.; Sudo, R.; Kamm, R.D.; Chung, S. In vitro 3D collective sprouting angiogenesis under orchestrated ANG-1 and VEGF gradients. *Lab Chip* 2011, 11, 2175–2181.
77. Kim, S.; Chung, M.; Ahn, J.; Lee, S.; Jeon, N.L. Interstitial flow regulates the angiogenic response and phenotype of endothelial cells in a 3D culture model. *Lab Chip* 2016, 16, 4189–4199.
78. Gadde, M.; Phillips, C.; Ghouseifam, N.; Sorace, A.G.; Wong, E.; Krishnamurthy, S.; Syed, A.; Rahal, O.; Yankeelov, T. E.; Woodward, W.A.; et al. In vitro vascularized tumor platform for modeling tumor-vasculature interactions of inflammatory breast cancer. *Biotechnol. Bioeng.* 2020, 117, 3572–3590.
79. Sobrino, A.; Phan, D.T.T.; Datta, R.; Wang, X.; Hachey, S.J.; Romero-López, M.; Gratton, E.; Lee, A.P.; George, S.C.; Hughes, C.C.W. 3D microtumors in vitro supported by perfused vascular networks. *Sci. Rep.* 2016, 6, 1–11.
80. Phillips, C.M.; Lima, E.A.B.F.; Woodall, R.T.; Brock, A.; Yankeelov, T.E. A hybrid model of tumor growth and angiogenesis: In silico experiments. *PLoS ONE* 2020, 15, e0231137.
81. Lima, E.A.B.F.; Oden, J.T.; Almeida, R.C. A hybrid ten-species phase-field model of tumor growth. *Math. Model. Methods Appl. Sci.* 2014, 24, 2569–2599.
82. Fritz, M.; Jha, P.K.; Köppl, T.; Oden, J.T.; Wohlmuth, B. Analysis of a new multispecies tumor growth model coupling 3D phase-fields with a 1D vascular network. *Nonlinear Anal. Real World Appl.* 2021, 61, 103331.
83. Fritz, M.; Jha, P.K.; Köppl, T.; Tinsley Oden, J.; Wagner, A.; Wohlmuth, B. Modeling and Simulation of Vascular Tumors Embedded in Evolving Capillary Networks. *arXiv* 2021, arXiv:2101.10183v2.
84. Koch, T.; Flemisch, B.; Helmig, R.; Wiest, R.; Obrist, D. A multiscale subvoxel perfusion model to estimate diffusive capillary wall conductivity in multiple sclerosis lesions from perfusion MRI data. *Int. J. Numer. Method. Biomed. Eng.* 2020.
85. D'Angelo, C. Multiscale modelling of metabolism and transport phenomena in living tissues. Lausanne EPFL 2007.
86. D'Angelo, C.; Quarteroni, A. On the coupling of 1D and 3D diffusion-reaction equations. Application to tissue perfusion problems. *Math. Model. Methods Appl. Sci.* 2008, 18, 1481–1504.
87. Köppl, T.; Vidotto, E.; Wohlmuth, B. A 3D-1D coupled blood flow and oxygen transport model to generate microvascular networks. *Int. J. Numer. Method. Biomed. Eng.* 2020, 36, e3386.
88. Hinow, P.; Gerlee, P.; McCawley, L.J.; Quaranta, V.; Ciobanu, M.; Wang, S.Z.; Graham, J.M.; Ayati, B.P.; Claridge, J.; Swanson, K.R.; et al. A Spatial Model of Tumor-Host Interaction: Application of Chemotherapy. *Math. Biosci. Eng.* 2009, 6, 521–546.
89. Swanson, K.R.; Rockne, R.C.; Claridge, J.; Chaplain, M.A.; Alvord, E.C.; Anderson, A.R.A. Quantifying the role of angiogenesis in malignant progression of gliomas: In silico modeling integrates imaging and histology. *Cancer Res.* 2011, 71, 7366–7375.
90. Hawkins-Daarud, A.; Rockne, R.C.; Anderson, A.R.A.; Swanson, K.R. Modeling tumor-associated edema in gliomas during anti-angiogenic therapy and its impact on imageable tumor. *Front. Oncol.* 2013, 3, 66.
91. Kohandel, M.; Kardar, M.; Milosevic, M.; Sivaloganathan, S. Dynamics of tumor growth and combination of anti-angiogenic and cytotoxic therapies. *Phys. Med. Biol.* 2007, 52, 3665–3677.
92. Kremheller, J.; Vuong, A.T.; Schrefler, B.A.; Wall, W.A. An approach for vascular tumor growth based on a hybrid embedded/homogenized treatment of the vasculature within a multiphase porous medium model. *Int. J. Numer. Method. Biomed. Eng.* 2019, 35, e3253.
93. Vidotto, E.; Koch, T.; Köppl, T.; Helmig, R.; Wohlmuth, B. Hybrid Models for Simulating Blood Flow in Microvascular Networks. *Multiscale Model. Simul.* 2019, 17, 1076–1102.

94. Shipley, R.J.; Smith, A.F.; Sweeney, P.W.; Pries, A.R.; Secomb, T.W. A hybrid discrete-continuum approach for modelling microcirculatory blood flow. *Math. Med. Biol.* 2020, 37, 40–57.
95. Xu, J.; Vilanova, G.; Gomez, H. Full-scale, three-dimensional simulation of early-stage tumor growth: The onset of malignancy. *Comput. Methods Appl. Mech. Eng.* 2017, 314, 126–146.
96. Yankeelov, T.E.; Atuegwu, N.; Hormuth, D.A.; Weis, J.A.; Barnes, S.L.; Miga, M.I.; Rericha, E.C.; Quaranta, V. Clinically Relevant Modeling of Tumor Growth and Treatment Response. *Sci. Transl. Med.* 2013, 5, 187ps9.
97. Lima, E.A.B.F.; Oden, J.T.; Wohlmuth, B.; Shahmoradi, A.; Hormuth, D.A.; Yankeelov, T.E.; Scarabosio, L.; Horger, T. Selection and validation of predictive models of radiation effects on tumor growth based on noninvasive imaging data. *Comput. Methods Appl. Mech. Eng.* 2017, 327, 277–305.
98. Lorenzo, G.; Hormuth, D.A.; Jarrett, A.M.; Lima, E.A.B.F.; Subramanian, S.; Biros, G.; Oden, J.T.; Hughes, T.J.R.; Yankeelov, T.E. Quantitative in vivo imaging to enable tumor forecasting and treatment optimization. *arXiv* 2021, arXiv:2102.12602.
99. Hahnfeldt, P.; Panigrahy, D.; Folkman, J.; Hlatky, L. Tumor development under angiogenic signaling: A dynamical theory of tumor growth, treatment response, and postvascular dormancy. *Cancer Res.* 1999, 59, 4770–4775.
100. Benjamin, T.; Kevin, R.K.; Robert, J.; Titz, B.; Kozak, K.R.; Jeraj, R. Computational modelling of anti-angiogenic therapies based on multiparametric molecular imaging data. *Phys. Med. Biol.* 2012, 57, 6079.
101. Goel, S.; Duda, D.G.; Xu, L.; Munn, L.L.; Boucher, Y.; Fukumura, D.; Jain, R.K. Normalization of the vasculature for treatment of cancer and other diseases. *Physiol. Rev.* 2011, 91, 1071–1121.

Retrieved from <https://encyclopedia.pub/entry/history/show/29084>